Chapter 10
Air Circulation in Urban Areas

Annalisa Di Bernardino, Olga Palusci, Agnese Pini, Giovanni Leuzzi, Marco Cacciani, Armando Pelliccioni, and Paolo Monti

10.1 Introduction

From a fluid dynamic point of view, the airflow above the Earth's surface is comparable to that developing above an unevenly warm rough surface. On a large scale and away from the Earth's surface, winds are mainly governed by Coriolis and pressure forces. These forces affect the intensity and direction of the synoptic (or geostrophic) wind, which defines the boundary condition for the underlying boundary layer.

The wind speed at the surface must necessarily be zero due to the viscosity of the air. Exhaustive studies, observations and theories concerning atmospheric flows can be found in several textbooks including those of Stull (1988), Garrat (1992), Holton (1992) and Jacobson (2005).

Atmospheric flows can be classified according to the spatial scales of the phenomena involved and range from the planetary scale (>10,000 km) to the microscale (1 mm–1 km). These include the synoptic scale (500–10,000 km), the mesoscale (2–2000 km) and subsequent subdivisions such as the urban scale (1 m–100 km) encompassing towns and neighbouring areas, the district scale (10 m–1 km), the urban canyon scale (~10 m) and the human scale (1 cm–1 m). The physical

A. Di Bernardino · M. Cacciani
Dipartimento di Fisica, Università di Roma "La Sapienza", Rome, Italy
e-mail: annalisa.dibernardino@uniroma1.it; marco.cacciani@uniroma1.it

O. Palusci · A. Pini · G. Leuzzi · P. Monti (✉)
Dipartimento di Ingegneria Civile Edile e Ambientale, Università di Roma "La Sapienza", Rome, Italy
e-mail: olga.palusci@uniroma1.it; agnese.pini@uniroma1.it; giovanni.leuzzi@uniroma1.it; paolo.monti@uniroma1.it

A. Pelliccioni
INAIL-DIMEILA, Monte Porzio Catone, Italy
e-mail: a.pelliccioni@inail.it

M. Palme, A. Salvati (eds.), *Urban Microclimate Modelling for Comfort and Energy Studies*, https://doi.org/10.1007/978-3-030-65421-4_10

processes associated with these scales are complex, especially in the presence of reservoirs and mountain ranges and when chemical, biological, geological and physical transformations are considerable (Fernando et al. 2001).

The atmospheric boundary layer (ABL) structure is influenced by soil properties, e.g. aerodynamic roughness, emissivity, albedo, heat capacity, thermal conductivity and water availability. The set of these parameters determines the surface temperature, which, in turn, regulates long-wave radiation towards the space, molecular heat flux into the ground and turbulent exchanges of heat and water vapour with the overlying air. The ABL depth varies considerably over time and space (usually from 100 to 2000 m) and evolves with the diurnal cycle of the solar radiation (Fig. 10.1a). Over land surfaces in high-pressure regions, the ABL is generally subdivided into several layers. At the bottom, there is the surface layer (10–100 m deep), where the turbulent fluxes are approximately constant. Above, the convective (or well-mixed) boundary layer and the stable (or nocturnal) boundary layer characterize daytime and night-time hours, respectively (Fig. 10.1b).

Although terrain effects are present even in nominally flat areas, the ABL is broadly classified in literature into that existing over flat terrain and that existing over complex terrain. When the ground is neither flat nor uniform, the ABL can be modified in terms of heating, moisture and momentum. Typical examples are geographically generated local winds, e.g. slope flows and sea breezes (Simpson 1994) as well as urban heat island (UHI) circulations (e.g. Fan et al. 2019).

UHIs are defined as the warmth produced by cities (Oke 1982). They may form above an urban area during both daytime and night-time, showing peculiar characteristics with respect to the ABL generally existing in rural areas. The difference in terrain coverage between urban and rural areas is mainly responsible for night-time and daytime urban-rural temperature anomalies that can even exceed 10 °C in the case of large cities (e.g. Roth et al. 1989; Santamouris 2001; Ravanelli et al. 2018). Possible causes for UHI formation are (a) reduced vegetation and increased paved

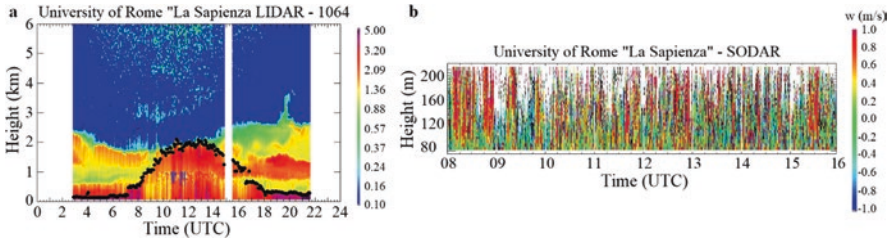

Fig. 10.1 (**a**) Example of LIDAR (light detection and ranging) scans of the backscattered light from the atmosphere on the 22nd of June 2005. The LIDAR is installed on the rooftop of the Department of Physics of the University of Rome "La Sapienza", Italy (Pichelli et al. 2014). The intensity of the backscatter (colour) is proportional to the aerosol concentration. The black dots denote the ABL height inferred from the backscatter vertical gradient. (**b**) Example of time history of the vertical velocity (w) profile measured by a SODAR (sonic detection and ranging) apparatus, placed next to the LIDAR. The features in red are signatures of thermals of warmer air rising from the ground during periods of strong convection, i.e. coherent vortical structures having diameter and depths of the order of the ABL depth (Stull 1988)

terrain that lower the potential for evapotranspiration which, in turn, implies that energy is converted into sensible rather than latent heat; (b) properties of urban materials, such as albedo, thermal emissivity, thermal conductivity and heat capacity; (c) urban geometry, which enhances the trapping of short- and long-wave radiations; and (d) anthropogenic heat (Oke 1982).

Knowledge of the wind flow structure within and above an urban area is of considerable interest in many respects, e.g. urban energy conservation (Blocken et al. 2011), air pollution (Ottosen et al. 2019), indoor air quality (Lai et al. 2015) and human comfort (Salvati et al. 2017b). Unfortunately, owing to the complexity of the geometric configurations involved, the wind flow is largely site dependent, thus limiting the application of simple models and formulations to predict wind flow in cities (Zajic et al. 2011).

This chapter illustrates the influence of city morphology on the flow field within urban areas. After a brief description of the gross features of ABLs above cities, the main characteristics of the wind flow around an isolated building and in correspondence with street canyons and groups of buildings are described and discussed.

10.2 Wind Flows Above Urban Canopies

Buildings and other urban infrastructure substantially change the dynamic and thermodynamic fields. Figure 10.2 shows a schematic of an urban environment and the modifications induced by buildings on the undisturbed wind.

Wind flow over an urban canopy, which is defined as the layer that extends from the ground up to the mean building height, is governed by the geometrical, thermal and radiative characteristics of the site. The urban boundary layer (UBL) is defined as the portion of the ABL between the surface and the height at which the underlying city no longer affects the airflow.

The similarity theory (Monin and Obukhov 1954) has given rise in the past to the profusion of considerable efforts in the search for general laws for average wind and air temperature profiles suitable for ABL analysis in the various stability conditions. Most studies reported in the literature show the considerable progress made hitherto, but also highlight the absolute shortage of laws valid in general for the urban environment.

The particular nature of city centres does not allow the development of robust parameterizations and theories for the velocity and temperature, as is the case of flat terrain, where the vertical profile of the average wind speed U reads

$$U = \frac{u_*}{k}\left[\ln\left(\frac{z}{z_0}\right) + \Psi\left(\frac{z}{L}\right)\right], \tag{10.1}$$

where z is the height, u_* the friction velocity (i.e. the scaling velocity, which is related to the drag force at the surface) and $k = 0.41$ the von Karman constant. L and

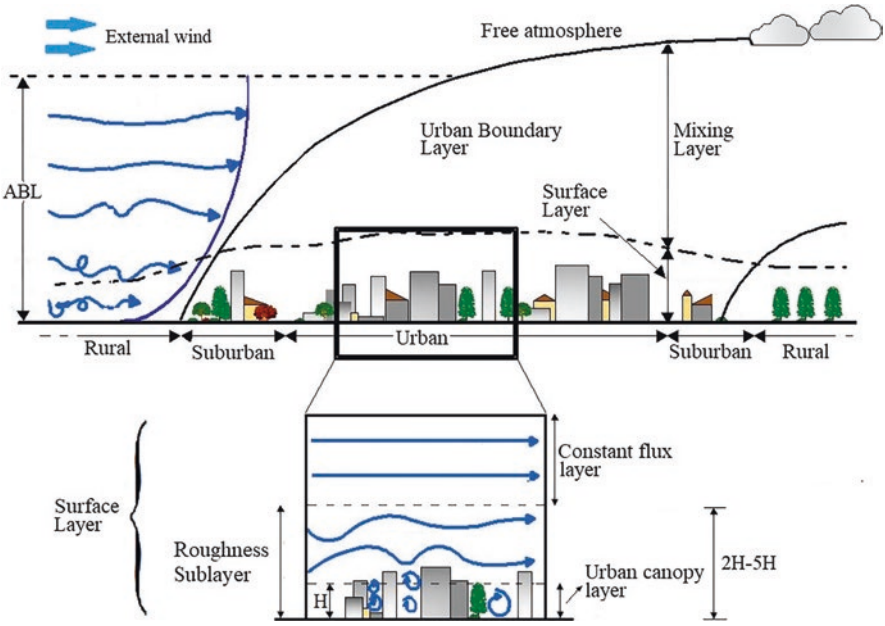

Fig. 10.2 Sketch of the UBL structure (modified from Fernando 2010)

z_0 are the Obukhov length and the aerodynamic roughness, respectively, and assume the role of scaling lengths. The latter is usually parameterized by means of descriptive land-use types (e.g. Britter and Hanna 2003), while L is proportional to the height above the surface at which buoyant factors first dominate over mechanical (shear) production of turbulence (e.g. Stull 1988). $\Psi(z/L)$ is a universal dimensionless function that equals zero in neutral conditions (Businger et al. 1971).

Conversely, an open question is the determination of the wind speed profile above cities. For example, within the roughness sublayer, i.e. the portion of the UBL immediately above the urban canopy (Fig. 10.3), Eq. (10.1) is not applicable. In such sublayer, the flow is three-dimensional, non-homogeneous and strongly influenced by vegetation, buildings and other roughness elements that constitute the urban canopy (Rotach 1999). Above urban or vegetation canopies, a region of constant flux generally exists (the constant flux layer), and Eq. (10.1) now assumes the form

$$U = \frac{u_*}{k}\left[\ln\left(\frac{z-d_0}{z_0}\right)+\Psi\left(\frac{z}{L}\right)\right], \tag{10.2}$$

where d_0 is the displacement height, i.e. the effective height of the ground due to the vertical flow displacement through the canopy. Both z_0 and d_0 are linked to the surface roughness elements. While u_* to be used in Eq. (10.2) is commonly measured within the constant flux layer, z_0 and d_0 are generally estimated by using the

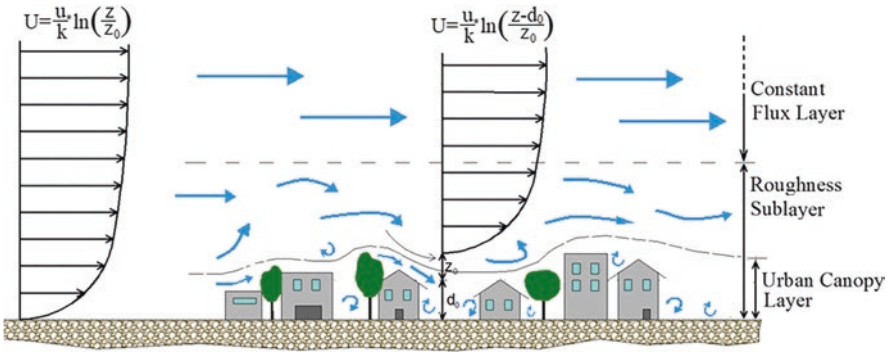

Fig. 10.3 Sketch of the wind profile above an urban area in neutral conditions (modified from Britter and Hanna 2003)

morphometric or anemometric method (Kent et al. 2017). In UBL studies, Eq. (10.2) is generally applied also within the roughness sublayer, where the condition of momentum flux constancy is never satisfied (Cheng and Castro 2002). An alternative formulation of (10.2) has been proposed recently by Pelliccioni et al. (2015), in which z_0 varies with height.

The picture described above is made even more complicated by the presence of complex terrain, in which airflows are mainly driven by local pressure gradients and thermal forcing (Whiteman 2000; Fernando 2010). This is the case of cities located, for example, in valleys surrounded by mountains (e.g. Giovannini et al. 2011, 2013), in which the airflow is determined mainly by terrain-induced perturbations to geostrophic flow (e.g. Valerio et al. 2017), or in coastal areas (e.g. Zhou et al. 2019).

10.3 Field Campaigns, Laboratory Experiments and Numerical Modelling

In order to solve practical problems in urban fluid mechanics area, we have to comply with the turbulent nature of wind flows. Randomness and non-linearity are just two of the intrinsic characteristics of turbulence that make the solution of the governing equations of fluid flows impossible to achieve analytically. Nevertheless, in order to solve urban fluid mechanics problems, three methods have been developed: field experiments, laboratory measurements and numerical simulations.

Field experiments could be considered in principle the ideal method since they provide values of the meteorological variable collected in the site of interest. Moreover, data coming from measurement campaigns may also be used to validate numerical simulations and laboratory experiments. Measurement instruments can be classified as either direct sensors or remote sensors. The former are placed on instrument platforms (e.g. masts and towers) and measure the parameters of interest at the location of the sensor. The latter measure waves (electromagnetic or sound)

and can give information referred to points far away from the instrument location. Among the classical direct instruments, we find anemometers (wind velocity), thermometers (air temperature), hygrometers (humidity), barometers (air pressure) and radiometers (solar, air and Earth radiations). Meanwhile, SODAR and LIDAR (see Fig. 10.1) belong to the class of remote sensors.

It is worth noting that sensor siting (in addition to their cost and management problems) represents one of the critical factors of field experiments, especially in an urban environment, where there are air circulations with small spatial scales. Another critical aspect of the field measurements concerns the uncontrollability of boundary conditions and therefore the significance of the data, as it is composed of the superposition of many simultaneous effects and processes. We can attempt to focus on one specific process by the careful selection of a weather pattern (e.g. fair weather). In this regard, it is necessary to consider that a measurement station within the urban canopy layer is dominated by microscale processes. It would be advisable to avoid siting in parks, if the aim is to collect data representative of the urban area. The choice of a location that is not affected by microclimatic effects too site-specific is essential.

Another important problem is the repeatability, which strictly does not occur in reality. In this respect, field measurements are fundamentally different from laboratory experiments and computational fluid dynamics (CFD), in which the boundary conditions can be easily controlled and repeatability should be straightforward. The variability and uncontrollability of field measurement conditions imply that validation of laboratory results and CFD simulations with field measurements only makes sense when the latter have been obtained based on quasi-steady boundary conditions (e.g. in the presence of persistent winds).

For years, laboratory simulations have been the only alternative to direct field measurements. They create an artificial turbulent domain in the laboratory (wind tunnel or water channel, see, e.g., Fig. 10.4), where only a limited number of processes or boundary conditions act on the flow. One of the advantages of using laboratory models lies in the fact that it is generally easy to control the boundary conditions as well as to investigate the role played by the non-dimensional variables governing the flow field. However, it should be noted that sometimes it is complicated (or even impossible) to attain the matching of non-dimensional parameters of models with their full-scale flow counterparts (e.g. Di Bernardino et al. 2015a). For example, the major restriction in laboratory simulations of the whole UHI is caused by the difficulty in reproducing the small UBL height–UHI diameter ratio observed in real UHIs (Lu et al. 1997; Cenedese et al. 2000). Further problems and limitations are due to the low Reynolds number (the ratio between inertial and viscous forces) attainable in the laboratory compared with that of real UHIs.

CFD is a well-established tool for solving urban fluid mechanics problems. Despite some drawbacks still present in its fundamental formulation (e.g. Rodi 1995), it is routinely employed to study wind flow and pollutant dispersion in urban areas (Blocken 2014). CFD solves the equations of fluid mechanics that describe the dynamics and thermodynamics of the gases in the atmosphere. Unlike analytical models, which provide a solution in each point of the domain, numerical models

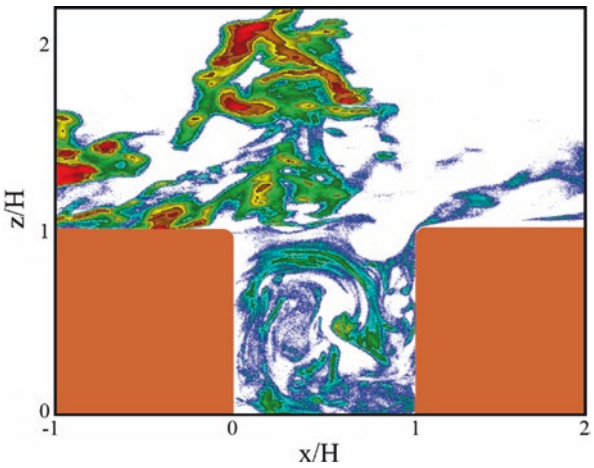

Fig. 10.4 Sketch of the instantaneous pollutant concentration field simulated in a water channel experiment simulating flow and dispersion in a street canyon. The flume is directed to the right. Each feature in brown represents a building $H = 2$ cm tall. The pollutant is emitted from a point source mimicking a chimney stack placed on the rooftop of one of the buildings located upwind of the building on the left (not included in the picture). The concentration is in arbitrary units (red refers to the maximum value, while white denotes zero). The pollutant enters the cavity mostly due to flow instability occurring at the interface between the cavity and the outer region (see Sect. 10.4.2) (the data set used refers to the experiment described in Di Bernardino et al. 2015b)

discretize the flow field to determine a solution only in discrete points of a numerical grid. The continuous differential equations that govern the flow field are approximated by a large number of algebraic equations describing local processes around the discrete points.

A number of different types of simulation approaches exist. Direct numerical simulation (DNS) solves all the scales of the turbulent fluctuating motions and the flow can be obtained in every detail of its very complex behaviour. Since only motions of scales larger than the mesh size can be resolved, the number of grid points required for solving the turbulent flow in the whole domain is too large and DNS cannot be used for practical applications in urban climate processes. Large eddy simulations (LES) and Reynolds-averaged Navier-Stokes (RANS) are the most common alternatives to DNS.

With RANS, all stochastic turbulent fluctuations are filtered out and only averaged equations are solved. In essence, only the mean flow field is explicitly solved and all scales of turbulence are modelled by solving additional balance equations for the closure (e.g. for the turbulence kinetic energy and its rate of dissipation). Large eddy simulations solve the large, energy-containing eddies in the flow field, which are usually anisotropic and contain most of the turbulence kinetic energy, while the small-scale eddies are modelled with a subgrid-scale model. LES intrinsically performs better than RANS and requires finer grids compared to RANS and therefore the computational cost is considerably higher.

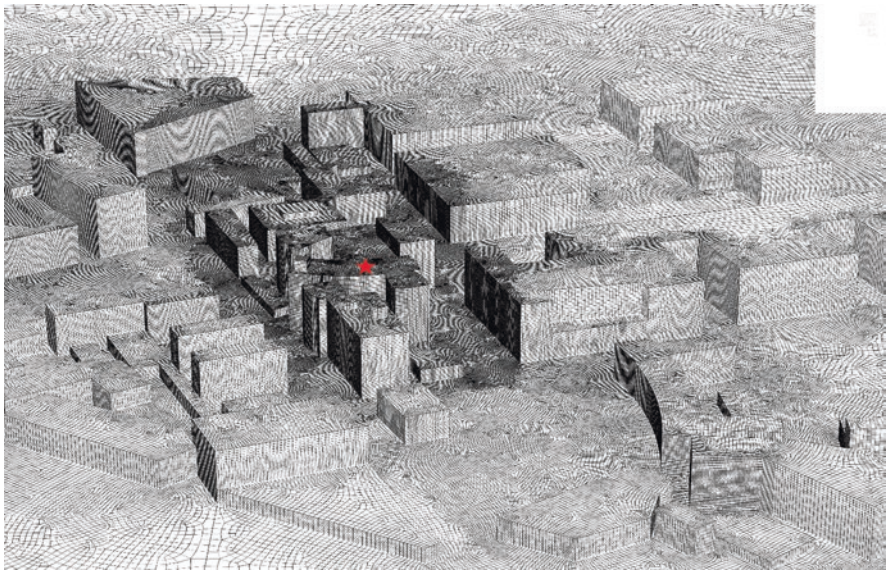

Fig. 10.5 CFD model of part of the Sapienza University of Rome. The planar area in the figure is about 1 km^2, while the maximum building height is 32 m. The grid was generated using the surface-grid extrusion technique (van Hooff and Blocken 2010) and consists of about 26.5×10^6 hexahedral cells. The red star denotes the building roof where the SODAR and LIDAR apparatus described in Fig. 10.1 are located

For more information on research methods currently used for urban fluid mechanics see the recent review by Moonen et al. (2012) (Fig. 10.5).

10.4 Wind Flow Inside Building Canopies

As mentioned above, airflow through real building canopies is extremely complex and depends on several geometrical parameters, e.g. arrangement and shape of the buildings, and thermal and radiative properties of the materials. Furthermore, it is also strongly affected by direction and turbulence characteristics of the approaching flow (Salizzoni et al. 2009, 2011).

Knowledge of how an isolated building or a group of buildings affect the local wind is important for several reasons; for example, it allows us (a) to estimate the way in which people could be buffeted by the wind at ground level or on aerial walkways; (b) to model concentration of pollutants emitted by urban sources (e.g. vehicles and chimneys); and (c) to analyse the influence of wind on heating and ventilating systems and thus to estimate their performance properly.

Although a few pioneering efforts to modelling the spatially averaged wind speed profile within the canopy have been proposed in the past (see, e.g., Cionco 1965; Macdonald 2000; Bentham and Britter 2002; Di Sabatino et al. 2008), the

complexity of the problem usually requires site-specific measurements performed by means of expensive field campaigns (e.g. Allwine et al. 2002), numerical simulations (e.g. Blocken 2015) or scaled physical models (e.g. Kastner-Klein and Rotach 2004). Alternatively, investigation of simple, basic configurations provides a useful contribution to the interpretation and physical comprehension of the basic mechanisms involved and can also give useful guidance for interpreting and sometimes estimating flows through real building canopies (Zajic et al. 2011).

10.4.1 Wind Past an Isolated Cubic Obstacle

The cube is the simplest idealization of a real building and it has been extensively investigated in the past both numerically and experimentally (e.g. Li and Meroney 1983; Martinuzzi and Tropea 1993; Murakami 1993; Snyder 1994; Santos et al. 2009; Tominaga and Stathopoulos 2010; Gousseau et al. 2011).

Despite the simple geometry, the flow pattern past a cube is very complex even when the approaching wind is perpendicular to one of the façades. The shear in the approaching wind causes a downward flow over the lower portion of the upwind façade of the building and a "horse-shoe vortex" at the upwind base, which wraps around the building near the ground extending also further downstream (Fig. 10.6). The flow separates at the upwind edges, producing separation zones on the rooftop and on the lateral sides of the building. At the downwind edges, the flow separates again, producing a cavity region and the associated bow vortex. The flow there interacts with the current merging from the roof and the sidewalls as well as with the horseshoe vortex. These vortex structures play a significant role in the physical processes governing pedestrian comfort and pollutant dispersion (e.g. Tominaga and Stathopoulos 2009; Bazdidi-Tehrani and Jadidi 2014). Their complex shape and structure should be considered in designing field campaigns in urban areas, where the siting and exposure of meteorological sensors are often, or to put it better, always, an incredibly complicated problem.

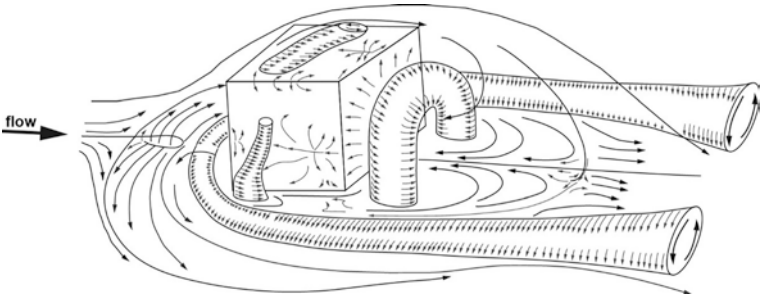

Fig. 10.6 Sketch of the flow pattern around an isolated building (modified from Martinuzzi 1992)

Figure 10.7 shows an example of the vector field of the mean velocity along a vertical plane passing through the centreline of a cubic obstacle. The eddy structure *A* refers to the bow vortex, while *B* is the signature of the horseshoe vortex located upstream of the cube. The recirculation region is about 1.3*H* long, where *H* is the building height and *R* the reattachment point. A third vortical structure (*C*) can also be seen and is located on the first half of the rooftop, while *S* is the stagnation point forming on the upwind façade.

The three panels in Fig. 10.8 show the mean concentration fields of a passive tracer emitted from a point source located upwind and downwind of the building

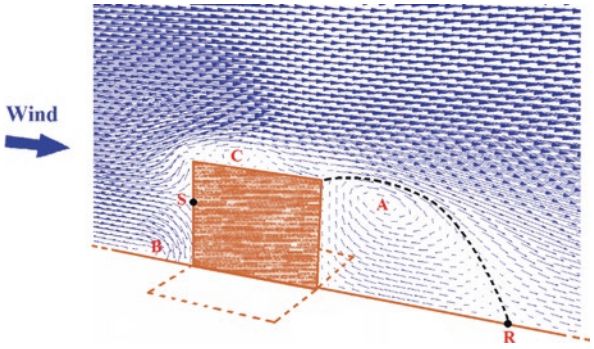

Fig. 10.7 Flow field around an isolated cubic obstacle. The approaching flow is directed rightward. Vectors indicate the velocity magnitude (in arbitrary units) along the vertical section parallel to the streamwise velocity passing through the obstacle centreline. The black dashed line refers to the upper limit of the recirculating region (the data set used refers to the water channel experiment described by Di Bernardino et al. 2017)

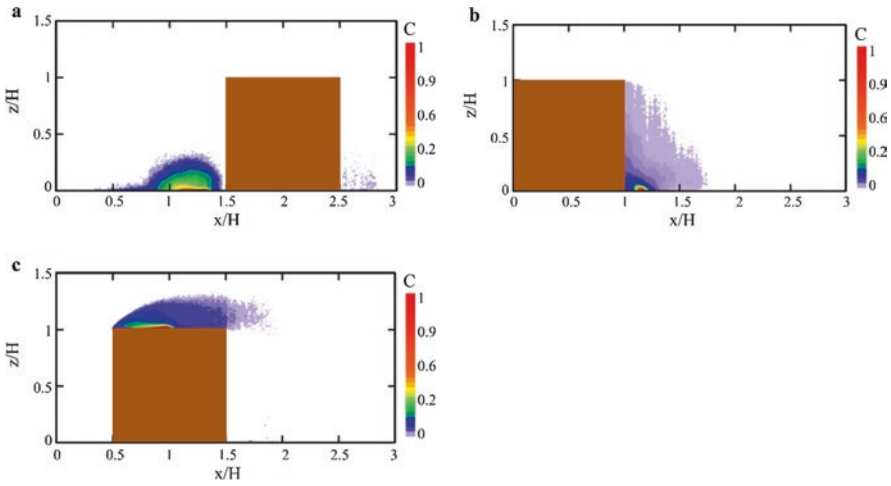

Fig. 10.8 Map of the mean concentration field C (in arbitrary units) of a passive tracer emitted from a point source located (**a**) upwind of the building, (**b**) in the lee of the building and (**c**) at the rooftop. The three panels refer to the same vertical section and data set of Fig. 10.7

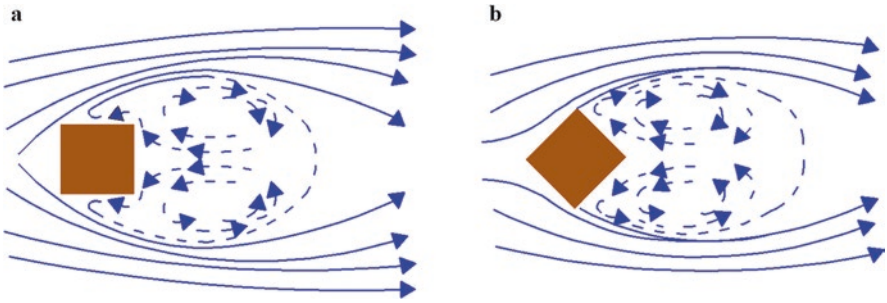

Fig. 10.9 Sketch of the flow patterns around an isolated cubic building along a horizontal plane in the case of approaching wind (**a**) perpendicular to a façade and (**b**) forming an angle of 45° with the façade (modified from Oke 1987)

and on the rooftop. Passive tracers have been extensively used in the past in identifying coherent structure in turbulent flows and can help in the flow analysis both in field campaigns (e.g. Leo et al. 2016) and in the laboratory (e.g. Pournazeri et al. 2012). When the source is upwind of the building (Fig. 10.8a), the pollutant is partially advected upstream and remains mainly trapped within the horseshoe vortex. Then, the tracer moves laterally and is carried downwind. Only a small part of the tracer penetrates into the cavity region in the lee of the building.

Similarly, when the tracer is emitted from the rooftop source (Fig. 10.8c), it remains on average confined in the vortex located in the upwind half of the cube top. For the case of the source located within the cavity region (Fig. 10.8b), the concentration field is quite different: the mean concentration shows much lower values because of the higher pollutant dilution caused by the bow vortex. Furthermore, the polluted plume moves upwind rising towards the upper levels of the building.

It is worthwhile remembering that the sketches depicted above can be considered representative only of cases of wind perpendicular to one of the façades. For all other wind directions, the airflow pattern changes dramatically and depends on the angle between the approaching flow and the façade (Fig. 10.9).

10.4.2 Wind in Street Canyons

The street canyon is defined as a geometric entity developed mainly along the street axis (in theory, of infinite length) and having the characteristic U-shape along the cross section. The street canyon is considered as an archetype for more complex and realistic urban geometries. One of the geometrical parameters to be considered is the aspect ratio $AR = H/W$, i.e. the ratio of the height of the buildings, H, to the spacing between buildings, W. Based on past studies conducted in wind tunnels and water channels, Oke (1987) summarized the nature of the flow in urban canopies in terms of AR (Fig. 10.10), viz. the skimming flow ($AR > 0.7$), in which a single vortex develops within the street canyon; the wake interference flow $0.3 < AR < 0.7$,

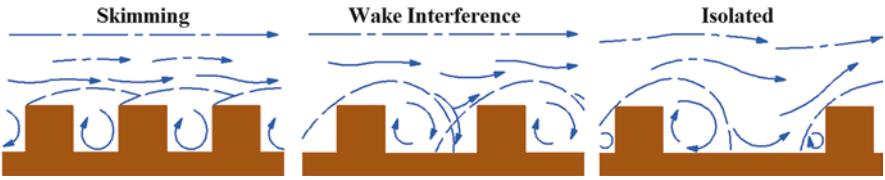

Fig. 10.10 Schematic of flow regimes for two-dimensional street canyons in the case of approaching wind perpendicular to the street axis (modified from Oke 1988)

which allows the development of two counterrotating vortexes; and the isolated obstacle regime ($AR < 0.3$), where the flow strictly resembles that observed for the isolated building case.

It is worth mentioning that the three flow conditions hold strictly in a neutrally stable atmosphere and when wind blows perpendicularly to the street axis. In all other cases, the flow pattern may change substantially due to wind canalization (e.g. Soulhac et al. 2008) and buoyancy effects. The latter can come into play when the wind speed is small (Kim and Baik 1999, 2001; Fernando 2010). Both these factors play an essential role in UHI dynamics (Martilli et al. 2002) and cannot be neglected in UBL modelling (e.g. Cantelli et al. 2015; Salvati et al. 2019).

A sketch of the wind circulation for the skimming flow with $AR = 1$ in the case of uniform building height is depicted in Fig. 10.11. The former is one of the archetypal flow configurations adopted in street flow studies (e.g. Baik et al. 2000; Kovar-Panskus et al. 2002) and represents the basic flow field for any further analysis concerning more realistic canyon geometry. The external wind (from left to right) flows almost parallel to the building rooftop above the canopy and separates from the flow inside the cavity, within which a main vortex forms. A counterrotating recirculating region located in the upper part of the façade of the leeward building and two other smaller vortices, located at the bottom corners of the canyon, complete the flow picture (see also Fig. 10.12 for a sketch of the average velocity streamlines). The instantaneous concentration field depicted in Fig. 10.11a highlights the Kelvin–Helmholtz billowing at the cavity top, triggered by dynamic instability that, in turn, is generated by the high shear levels at the top of the canyon. These billows govern mass and momentum transfer between the cavity and the external flow (see, e.g., Jaroslawski et al. 2019 and references cited therein).

The interaction between canyon and outer flow is greater for the wake interference regime, where the size of the secondary vortex located at the bottom of the leeward building grows with AR (e.g. Ferrari et al. 2017). Flow separation at the cavity top is however still present. Case $AR = 0.5$ shows two well-defined adjacent vortices: the downstream one is by far the larger and rotates clockwise, while the upstream one is smaller, occupying nearly one-fourth of the canyon and rotating counterclockwise (Fig. 10.12). For this geometry, the outer flow has difficulty in penetrating the inter-element space. As a result, it skims and remains nearly parallel to the roofs, thus preventing the formation of the recirculating region at the building top seen previously for the isolated cubic building (Figs. 10.6 and 10.7). This

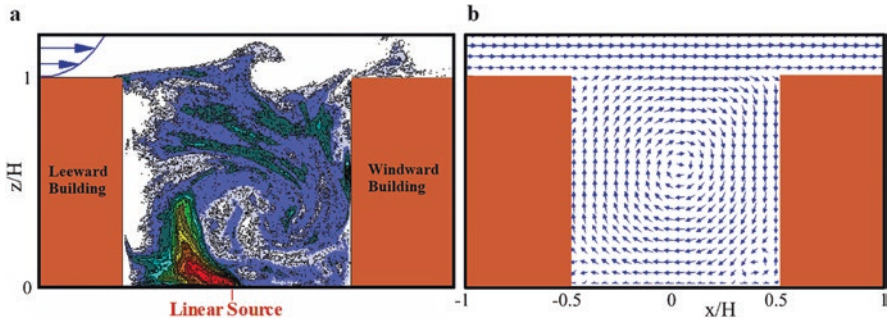

Fig. 10.11 (**a**) Colour map of the instantaneous concentration field (in arbitrary units; red is the maximum concentration value, white indicates zero) of a pollutant emitted from a linear source at ground level within an $AR = 1$ street canyon. (**b**) As in (**a**), but for the mean velocity vectors (in arbitrary unit). The external flow is rightward (the data set used refers to the water channel experiments described by Di Bernardino et al. 2018)

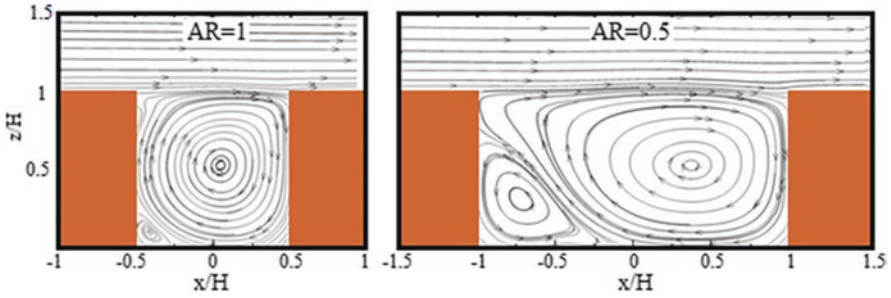

Fig. 10.12 Examples of streamlines of the mean velocity. The external flow comes from the left (adapted from Nardecchia et al. 2018)

feature causes poor canyon ventilation, even for strong external winds, and it is one of the main causes of air quality deterioration and air stagnation in cities. Canyon ventilation is essentially governed by the dynamics of the shear layer at the canyon top, which forms because of the large velocity gradients occurring in this area (see also Fig. 10.4). The shear layer plays a key role in the exchange of air and scalars between the canopy and the overlying region (Louka et al. 2000; Takimoto et al. 2011; Di Bernardino et al. 2018).

Similarly to what happens in the case of isolated building flows, wind direction plays a significant role in the flow field inside the cavity. In principle, if the external wind has a component along the street axis, the flow topology changes dramatically within the canyon. It is no longer two-dimensional and is characterized by an irregular helix (Fig. 10.13).

The main difference with the case of the approaching wind perpendicular to the street axis is the presence of a wind component parallel to the street axis itself. This channelling effect increases close to the ground and causes the progressive

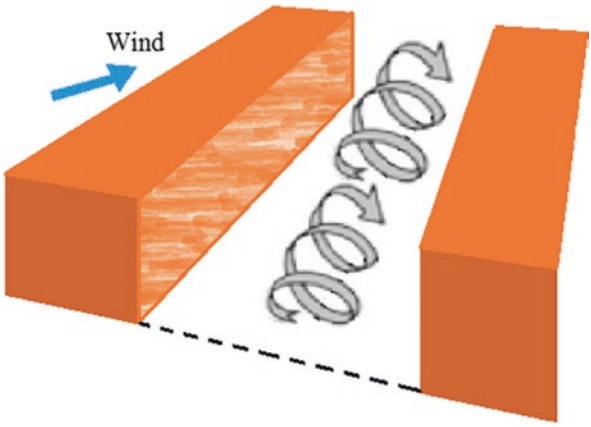

Fig. 10.13 Sketch of flow topology inside a street canyon in the case of external wind not perpendicular to the street axis

reduction of the angle between the wind direction and the street axis (see, e.g., Soulhac et al. 2008 and references cited therein). Another parameter to be taken into account is the canyon asymmetry, that is, the ratio between the heights of the buildings facing the streets. The asymmetry of the canyon has different effects on the airflow, pollutant dispersion and thermal comfort (Baik et al. 2000).

We conclude this section by observing that aspect ratios $AR = 1$ and 0.5 do not cover all possible situations found in real urban area, not even with regard to archetypal street canyon shapes (Ratti et al. 2006; Salvati et al. 2017a, b; Badas et al. 2019). It is therefore useful to analyse other street canyon geometries and to describe their characteristics separately.

10.4.2.1 Effects of Aspect Ratio and Building Rooftop Shape

In principle, a decrease in AR is accompanied by an increase in canyon ventilation, and vice versa. Figure 10.14 illustrates the streamlines of the average velocity for three skimming flow configurations. While for $AR = 1.33$ no substantial differences with $AR = 1$ appear, further increases of AR give rise to multi-vortex configurations (see Zajic et al. 2011 and references cited therein). For $AR = 2$, the two vortices at the bottom seen for $AR = 1.33$ merge to form a larger counterclockwise structure. Two large separated regions therefore appear inside the canyon. Further increases in AR lead to the formation of additional vortices.

For example, for $AR = 4$ three vortices form, with the lowest of them of smaller size. The configuration of narrow canyons is particularly interesting for the investigation of dispersion phenomena and air ventilation (e.g. Cheng and Liu 2011) in that the bottom region is practically disconnected from the outer flow. In essence, the narrow the street canyon the lower the canyon ventilation. For this reason, it is fundamental to consider a correct urban planning to minimize the unwanted effects of pollutant accumulation or air stagnation.

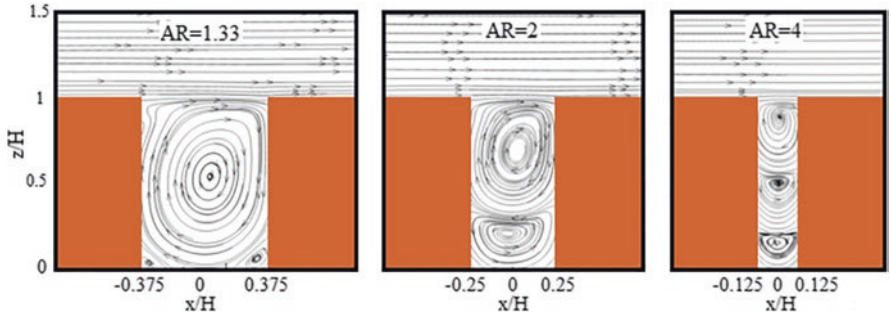

Fig. 10.14 Streamlines of the mean velocity magnitude for the skimming flow regime. The external flow comes from the left (adapted from Nardecchia et al. 2018)

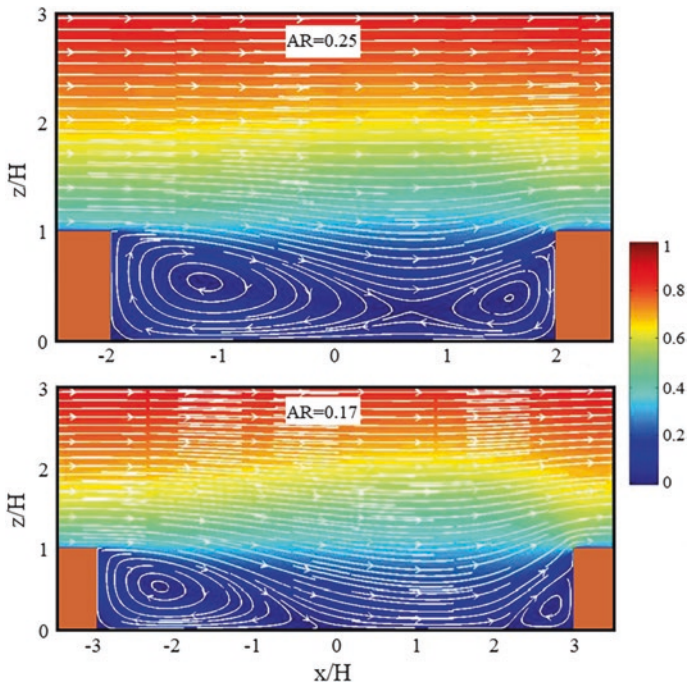

Fig. 10.15 Examples of the mean velocity magnitude normalized with the free stream velocity for the isolated flow regime (colours). The lines denote streamlines (adapted from Badas et al. 2017)

In contrast, reductions in the value of AR are accompanied by a progressive increase in canyon ventilation. Figure 10.15 shows velocity maps obtained numerically by Badas et al. (2017) for $AR = 0.25$ and 0.17 (colours represent mean velocity magnitude made non-dimensional by the free stream velocity). Although both of them are considered as belonging to the isolated flow regime ($AR < 0.3$), the two maps show that the two vortical structures within the canyon are in the first case still

interconnected to each other as we would have expected for the wake interference regime ($0.3 < AR < 0.7$). However, the vortex in the lee of the upwind building is considerably longer in both the geometries.

One of the parameters mostly used in evaluating air quality and human comfort at street level is the air exchange rate, *ACH*, i.e. the rate of air removal from a street canyon. Owing to the flow two-dimensionality, *ACH* is equal to the mean upward velocity at the canyon top (Liu et al. 2005). By definition, the larger the *ACH* the better the canyon ventilation. Badas et al. (2017) calculated the *ACH* for the arrangements shown in Fig. 10.15 plus other 21 geometries for 23 cases, which include *AR* values ranging between 0.07 (isolated flow regime) and 3 (multi-vortex skimming flow regime). The ACH shows relatively large values for low aspect ratios, a region of low values for large *AR*, where it is about ¼ compared to the maxima, and an intermediate trend in between (Fig. 10.16).

Badas et al. (2017) also focused on assessing the effect of gable roofs on the flow regimes and their implications in terms of *ACH*. Their results corroborated the idea that a pitched roof strongly modifies the low-level flow and increases the turbulence and the air exchange between the canyon and the external flow (see Ferrari et al. (2019) for a discussion on the effect of the shape of buildings and chimney stacks on ventilation and pollutant dispersion). In particular, they found that the pitch has a positive effect on *ACH* both in the high and low aspect ratio ranges. Such a growth is particularly significant (even a factor of three) in the range of narrow canyons, mainly because of the larger contribution of the mean flow compared to that present in the case of a flat roof (Fig. 10.17). Note that the curves of *ACH* collapse onto a single curve in the intermediate, descending range of aspect ratios.

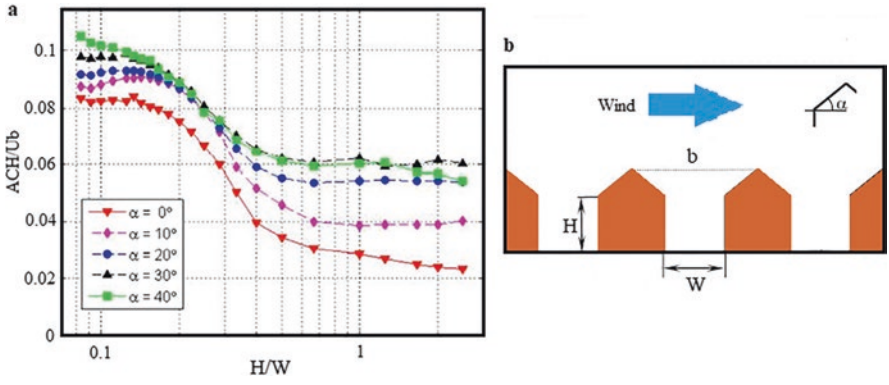

Fig. 10.16 (**a**) Non-dimensional *ACH* versus *H*/*W* for two-dimensional street canyons with planar rooftop (roof slope $\alpha = 0^{\circ}$, red line). The other curves refer to *ACH* calculated for different α. *U* indicates the free stream velocity. (**b**) Sketch of the computational domain (adapted from Badas et al. 2017)

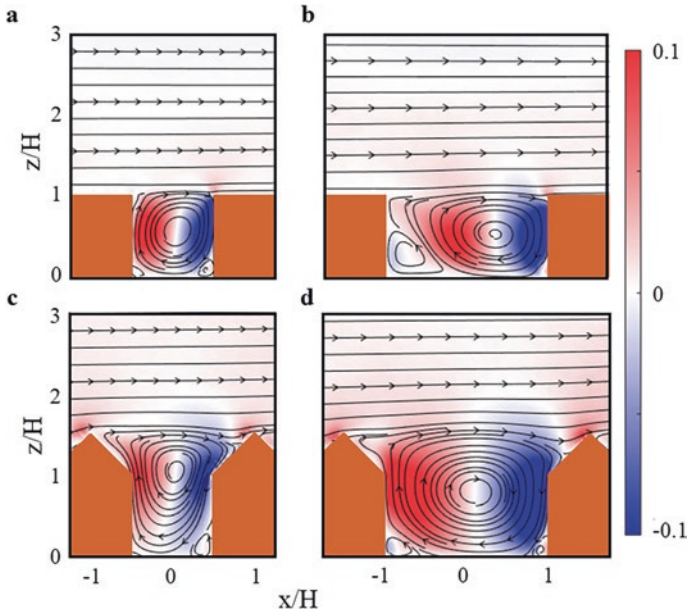

Fig. 10.17 Streamlines of the mean velocity field for different aspect ratios and roof shapes. Colours indicate the vertical wind velocity component made non-dimensional by the free stream velocity for (**a**) $AR = 1$ and $\alpha = 0$, (**b**) $AR = 0.5$ and $\alpha = 0$, (**c**) $AR = 1$ and $\alpha = 45°$ and (**d**) $AR = 0.5$ and $\alpha = 45°$ (adapted from Garau et al. 2018)

10.4.2.2 Effect of Building Height Variation

The role played in the flow topology by the ratio between the height of the windward and the leeward building, $R = H_W/H_L$, has been extensively investigated in the past (e.g. Zajic et al. 2011 and references cited therein). With regard to the case of flat rooftops, Nardecchia et al. (2018) focused on the combined effect of the variability of both R and AR by considering six values of R and five ARs. In particular, they analysed the step-up configurations, where the leeward building ($H_L < H_W$) is shorter than the windward building, and the step-down configurations ($H_L > H_W$). Figure 10.18 shows examples of streamlines for step-up (R = 1.5, 2 and 2.5) and step-down (R = 0.67, 0.5 and 0.4) geometries and AR = 0.5, 1.5 and 4.

For the step-up configurations ($R > 1$) for $AR = 0.5$ and 1.5 the flow fields do not change much from that seen for $R = 1$ (Fig. 10.11). The main vortex increases in size and moves upward as R grows. Regarding the skimming flow cases for $AR = 1.5$, their dependence on R is definitely greater. There is a progressive ejection of the upper vortex from the canyon into the overlying layer going from $R = 1.5$ to 2.5. In terms of air ventilation, this is reflected in the fact that ACH does not depend significantly on R when $AR = 0.5$ and 1 (Fig. 10.19), while a clear decrease in ACH for increasing R occurs for the other aspect ratios. Taller windward buildings allow lower vertical mass transfer between the canyon and the overlying region. On the

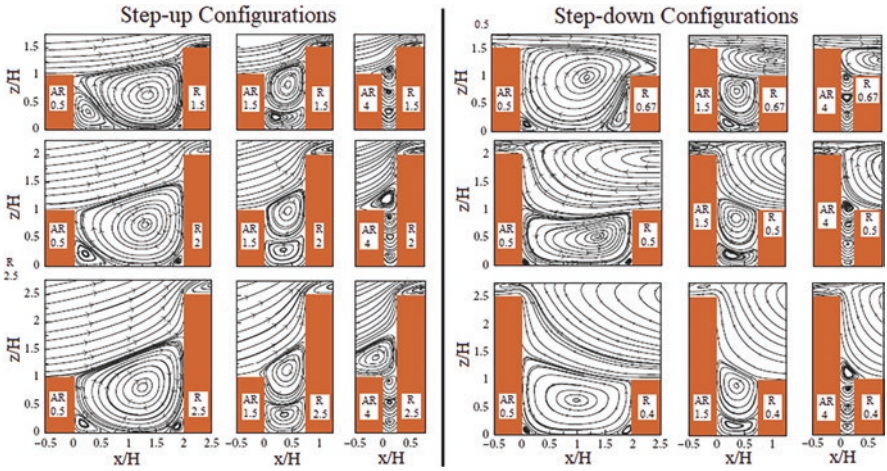

Fig. 10.18 Streamlines of the mean velocity for different aspect ratios (*AR*) and relative height (*R*) of the buildings (adapted from Nardecchia et al. 2018)

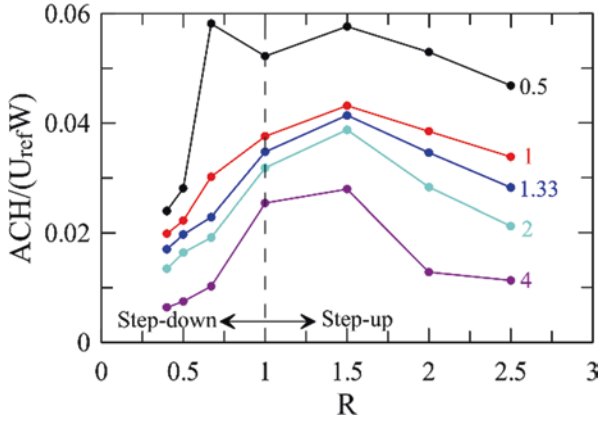

Fig. 10.19 Non-dimensional *ACH* versus *R*. Numbers near the curves denote *AR* (adapted from Nardecchia et al. 2018)

other hand, the step-down configurations ($R < 1$) show a wide clockwise vortex placed over the canyon and the top of the windward building. Overall, the lower the *R* the smaller the *ACH*, with the exception of the case ($AR = 0.5 - R = 0.67$) for which there is only a large vortical structure that occupies both the canyon and the overlying region up to $z = H_L$. The latter configuration corresponds with the largest *ACH* calculated for all the cases analysed. In contrast, for all the other step-down configurations, the main vortex (or the two or more vortices) remains confined within the canyon. The latter represents the main difference between step-up and step-down configurations and it certainly has great influence on pollutant concentration, particularly at street level.

From the point of view of air quality analysis, the development of secondary vortices in the lower corners of the canyon for $AR = 0.5$ and 1 should determine an accumulation of pollutants near the sidewalk, regardless of R. For $AR = 1.5$ and 2, the presence of the two counterrotating vortices further limits the canyon ventilation, especially at ground level. For $AR = 4$, the vertically aligned multiple vortex configuration strongly inhibits the exchange of air with the higher layers and paves the way to stagnation of pollutants at pedestrian level.

We conclude this subsection by showing the effects on the flow pattern of street canyons having flat roof on one street side and gable roofs on the opposite side. The results found numerically for several rooftop geometries by Xie et al. (2005a, b) show a substantial resemblance of A and B cases to the step-up and step-down configurations seen above for $AR = 1$ and $R = 1.5$ and 0.67, respectively (Fig. 10.20). On the other hand, cases C and D show quite clearly the role played by the approaching wind direction even in cases of winds perpendicular to the street axis. This fact is further evidence that the knowledge of prevailing winds can be extremely useful during earlier design stage.

10.4.3 Groups of Buildings

As mentioned earlier, the turbulent nature of the urban flow makes it impossible to analytically solve the wind field in urban environments. Similarly to the street canyon case, most CFD and laboratory studies on groups of buildings consider idealized situations like the regular arrangement of obstacles depicted in Fig. 10.21a, i.e. an approaching wind perpendicular to the façades of a group of regular cubes mimicking a real urban complex. Usually, the geometrical parameters used to classify

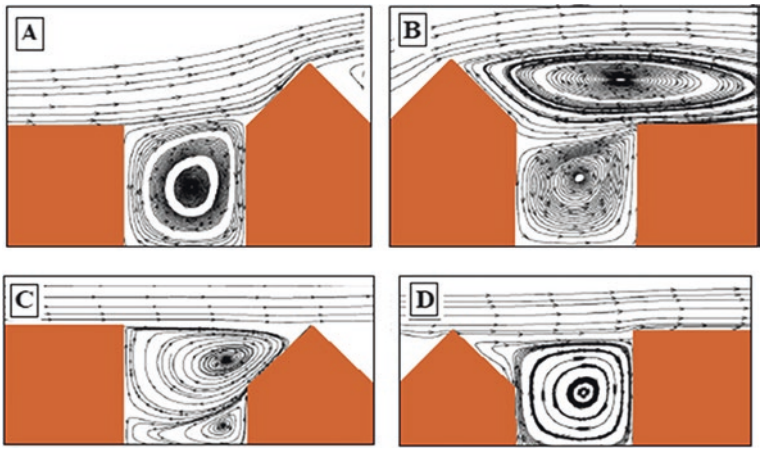

Fig. 10.20 Influence of roof shape on streamlines in street canyon (adapted from Xie et al. 2005a, b)

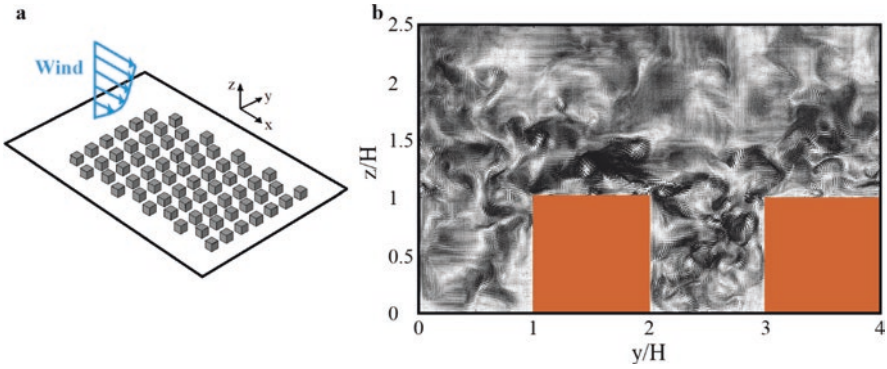

Fig. 10.21 (**a**) Sketch of archetypal array of cubes usually adopted in CFD simulations and laboratory experiments and (**b**) instantaneous snapshot of the velocity field in a vertical y–z plane perpendicular to the approaching mean flow (which is out of the page) obtained for a staggered building array with $\lambda_P = 0.25$ by means of a DNS (adapted from Coceal et al. 2006)

urban canopies are the plan area density, λ_P, and the frontal area density, λ_F, defined, respectively, as the plan area and frontal area occupied by buildings divided by the total area of the land on which they are located. We remind the reader that λ_P and λ_F are just two of the several parameters involved in urban canopy classification. For additional information see Grimmond and Oke (1999), Ratti et al. (2006) and Stewart and Oke (2012).

The instantaneous snapshot of the velocity field depicted in Fig. 10.20b helps to elucidate the complexity of the turbulent flow within a group of staggered buildings. The wind field is strongly inhomogeneous and vortical structures (with circulation in both clockwise and counterclockwise sense) are present throughout the flow. In terms of average quantities, the velocity pattern is undoubtedly simpler in so much that the averaging over many instantaneous realizations filters out small-scale structures in the flow pattern and emphasizes the main flow features.

Figure 10.22 depicts the average velocity field referred to the same simulation of Fig. 10.21, but for a vertical x–z plane—which is parallel to the streamwise velocity—passing through the centre of the buildings (Coceal et al. 2006). The main feature is the recirculation region in the bottom right-hand corner in front of the windward building. Such vortical structure is rather persistent and is accompanied by a strong downdraft down the façade. Note the absence of a recirculation behind the leeward building, while there is a clear reverse flow near the bottom surface between $x/H = 1$ and 2 and a strong updraft adjacent to the back façade similar to that observed for the isolated building. It is also worthwhile noticing that a recirculation vortex appears in the lower part of the canopy if one considers the vertical planes parallel to the one above (not shown). This fact is a further evidence of the strong three-dimensionality of the flow (for more details see Coceal et al. 2006).

The flow complexity is even clearer by looking at the streamlines (Fig. 10.23) corresponding to the horizontal average velocity referred to an aligned cube array for two external wind directions (0° and 45°) and a staggered array for 45° (Coceal

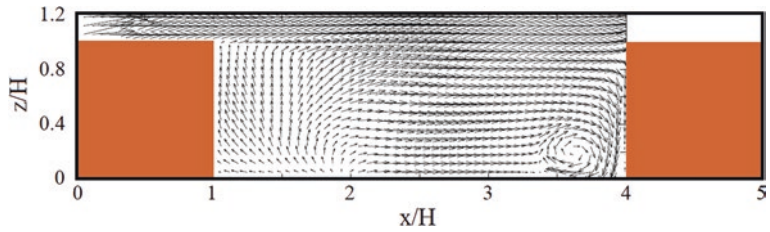

Fig. 10.22 Average velocity field in a vertical x–z plane through the middle of the cubes of the array in Fig. 10.21. The streamwise velocity is now directed rightward (adapted from Coceal et al. 2006)

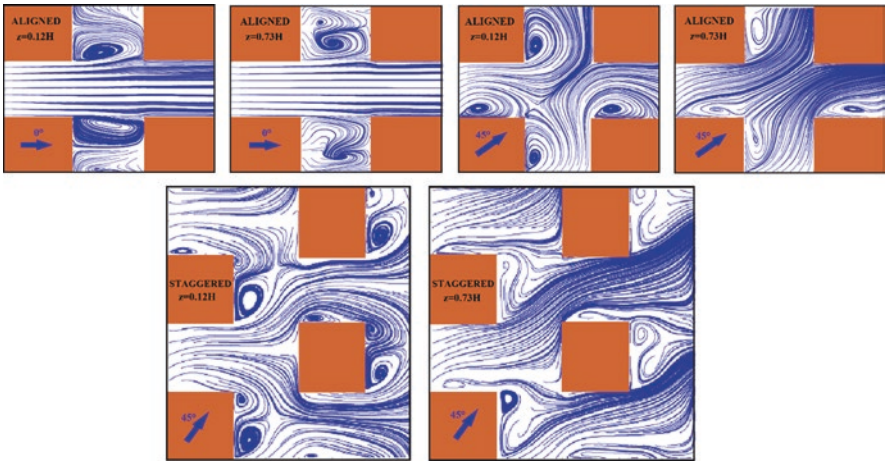

Fig. 10.23 Streamlines along horizontal planes for aligned and staggered regular arrays of cubical buildings for two directions of the approaching flow (adapted from Coceal et al. 2014)

et al. 2014). Streamlines are plotted at $z = 0.12H$ (i.e. close to pedestrian level) and $0.73H$ for each configuration. The large recirculation within the canyon region behind each building and the channelling in the street aligned with the external velocity characterize the 0° flow. While the streamlines within the channelling region are similar at the two heights, the vortical structures behind the buildings are essentially three-dimensional and change considerably with height.

As shown by Kim and Baik (2004), the flow coming into the street canyon curls up around the so-called portal vortex, whose ends are located near the lower edges of the windward building (Fig. 10.24a). The portal vortex is symmetric with respect to the centre of the street canyon and its horizontal axis is perpendicular to the external wind direction. The same authors showed that for external winds not perpendicular to the façade, the horizontal size of the portal vortex changes and a horseshoe vortex forms around the façades of the leeward building. When the incident wind angle is 45°, the flow is diagonally symmetric behind the windward building (Fig. 10.24b).

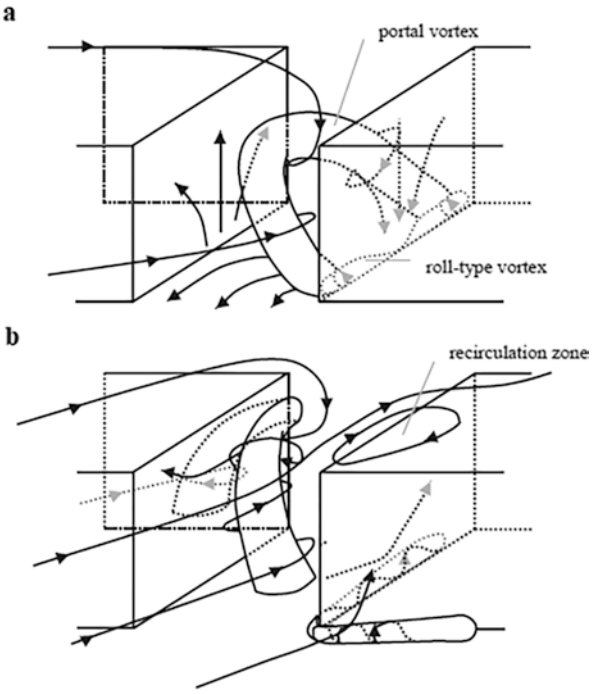

Fig. 10.24 Sketch of the mean flow circulation for external wind (**a**) perpendicular and (**b**) inclined of 45° with respect to the street axis (adapted from Kim and Baik 2004)

Streamlines for the external wind of 45° show the occurrence of a recirculation behind each façade. Such a feature reduces in size with height and is symmetrically situated with respect to the 45° diagonal line through the buildings. Streamlines from the two perpendicular streets upstream of the intersection come together and then diverge around the corner of the next building at the intersection, part of them feeding into a recirculation on the leeward face of the upstream buildings in the street perpendicular to the original flow direction and another part channelling into the far side of that same street. These flows play a considerable role in ventilation and in near-source dispersion as well (e.g. Coceal et al. 2014; Mei et al. 2017). For the external wind of 45° and staggered array, the pattern of streamlines is considerably more complicated. There is no longer symmetry with respect to the 45° diagonal line throughout the array and the flow topology is modified substantially.

10.5 Conclusions

The wind flows described in the preceding sections are only a limited part of cases that can be seen in real cities. Vegetation (e.g. trees and green roofs), canyon asymmetries, squares, viaducts as well as thermal inhomogeneity of the urban canopy layer are just some of the features normally found in cities that make the picture even more complicated and particularly difficult to generalize. Despite the

continuous effort of many researchers, the progressive lowering of the meteorological instrumentation costs, and the increase in computing power, the knowledge of wind circulation in cities is still far from being exhaustive. The lack of analytical laws that provide wind speed even in simple cases such as an isolated building is just one example of the complexity of the phenomenon. This must spur on the scientific community to enrich its knowledge of an important and fascinating topic such as urban fluid mechanics.

References

Allwine, K. J., Shinn, J. H., Streit, G. E., Clawson, K. L., & Brown, M. (2002). Overview of URBAN 2000: A multiscale field study of dispersion through an urban environment. *Bullettin of the American Meteorological Society, 83*, 521–536.

Badas, M. G., Ferrari, S., Garau, M., & Querzoli, G. (2017). On the effect of gable roof on natural ventilation in two-dimensional urban canyons. *Journal of Wind Engineering and Industrial Aerodynamics, 162*, 24–34.

Badas, M. G., Salvadori, L., Garau, M., Querzoli, G., & Ferrari, S. (2019). Urban areas parameterization for CFD simulations and cities air quality. *International Journal of Environment and Pollution, 66*, 5–18.

Baik, J.-J., Park, R.-S., Chun, H.-Y., & Kim, J.-J. (2000). A laboratory model of urban street canyon flows. *Journal of Applied Meteorology, 39*, 1592–1600.

Bazdidi-Tehrani, F., & Jadidi, M. (2014). Large eddy simulation of dispersion around an isolated cubic building: Evaluation of localized dynamic k_{SGS}-equation sub-grid scale model. *Environmental Fluid Mechanics, 14*, 565–589.

Bentham, T., & Britter, R. E. (2002). Spatially averaged flow velocity within large groups of obstacles. *Atmospheric Environment, 37*, 2037–2043.

Blocken, B. (2014). 50 years of computational wind engineering: Past, present and future. *Journal of Wind Engineering and Industrial Aerodynamics, 129*, 69–102.

Blocken, B. (2015). Computational fluid dynamics for urban physics: Importance, scales, possibilities, limitations and ten tips and tricks towards accurate and reliable simulations. *Building and Environment, 91*, 219–245.

Blocken, B., Stathopoulos, T., Carmeliet, J., & Hensen, L. M. (2011). Application of computational fluid dynamics in building performance simulation for the outdoor environment: An overview. *Journal of Building Performance Simulation, 4*, 157–184.

Britter, R. E., & Hanna, S. (2003). Flow and dispersion in urban areas. *Annual Review of Fluid Mechanics, 35*, 469–496.

Buccolieri, R., Salizzoni, P., Soulhac, L., Garbero, V., & Di Sabatino, S. (2015). The breathability of compact cities. *Urban Climate, 13*, 73–93.

Businger, J. A., Wyngaard, J. C., Izumi, Y., & Bradley, E. F. (1971). Flux-profile relationships in the atmospheric surface layer. *Journal of the Atmospheric Sciences, 28*, 181–189.

Cantelli, A., Monti, P., & Leuzzi, G. (2015). Numerical study of the urban geometrical representation impact in a surface energy budget model. *Environmental Fluid Mechanics, 15*, 251–273.

Cenedese, A., Miozzi, M., & Monti, P. (2000). A laboratory investigation of land and sea breeze regimes. *Experiments in Fluids, 29*(Suppl. 1), S291–S299.

Cheng, H., & Castro, I. P. (2002). Near wall flow over urban-like roughness. *Boundary-Layer Meteorology, 104*, 229–259.

Cheng, W. C., & Liu, C.-H. (2011). Large-eddy simulation of flow and pollutant transports in and above two-dimensional idealised street canyons. *Boundary-Layer Meteorology, 139*, 411–437.

Cionco, R. M. (1965). Mathematical model for air flow in a vegetative canopy. *Journal of Applied Meteorology, 4*, 517–522.

Coceal, O., Thomas, T. G., Castro, I. P., & Belcher, S. E. (2006). Mean flow and turbulence statistics over groups of urban-like cubical obstacles. *Boundary-Layer Meteorology, 121*, 491–519.

Coceal, O., Goulart, E. V., Branford, S., Thomas, T. G., & Belcher, S. E. (2014). Flow structure and near-field dispersion in arrays of building-like obstacles. *Journal of Wind Engineering and Industrial Aerodynamics, 125*, 52–68.

Di Bernardino, A., Monti, P., Leuzzi, G., & Querzoli, G. (2015a). On the effect of the aspect ratio on flow and turbulence over a two-dimensional street canyon. *International Journal of Environment and Pollution, 58*, 27–38.

Di Bernardino, A., Monti, P., Leuzzi, G., & Querzoli, G. (2015b). Water-channel study of flow and turbulence past a 2D array of obstacles. *Boundary-Layer Meteorology, 155*, 73–85.

Di Bernardino, A., Monti, P., Leuzzi, G., Sammartino, F., & Ferrari, S. (2017). Experimental investigation of turbulence and dispersion around an isolated cubic building. Proc. 18th Int. Conf. Harmonisation within Atmospheric Dispersion Modelling for Regulatory Purposes, 9–12 October, Bologna, Italy.

Di Bernardino, A., Monti, P., Leuzzi, G., & Querzoli, G. (2018). Pollutant fluxes in two-dimensional street canyons. *Urban Climate, 24*, 80–93.

Di Sabatino, S., Solazzo, E., Paradisi, P., & Britter, R. (2008). A simple model for spatially-averaged wind profiles within and above an urban canopy. *Boundary-Layer Meteorology, 127*, 131–151.

Di Sabatino, S., Leo, L. S., Cataldo, R., Ratti, C., & Britter, R. E. (2010). Construction of digital elevation models for a southern European city and a comparative morphological analysis with respect to northern European and North American cities. *Journal of Applied Meteorology and Climatology, 49*, 1377–1396.

Fan, Y., Hunt, J., Wang, Q., Yin, S., & Li, Y. (2019). Water tank modelling of variations in inversion breakup over a circular city. *Building and Environment, 164*, 106342.

Fernando, H. J. S. (2010). Fluid dynamics of urban atmospheres in complex terrain. *Annual Review of Fluid Mechanics, 42*, 365–389.

Fernando, H. J. S., Lee, S. M., Anderson, J., Princevac, M., Pardyjak, E., & Grossman-Clarke, S. (2001). Urban fluid mechanics: Air circulation and contaminant dispersion in cities. *Environmental Fluid Mechanics, 1*, 107–164.

Ferrari, S., Badas, M. G., Garau, M., Seoni, A., & Querzoli, G. (2017). The air quality in narrow two-dimensional urban canyons with pitched and flat roof buildings. *International Journal of Environment and Pollution, 62*, 347–368.

Ferrari, S., Badas, M. G., Garau, M., Salvadori, L., Seoni, A., & Querzoli, G. (2019). On the effect of the shape of the buildings and chimneystacks on ventilation and pollutant dispersion. *EPJ Web Conferences, 213*, 02017.

Garau, M., Badas, M. G., Ferrari, S., Seoni, A., & Querzoli, G. (2018). Turbulence and air exchange in a two-dimensional urban street canyon between gable roof buildings. *Boundary-Layer Meteorology, 167*, 123–143.

Garrat, J. R. (1992). *The atmospheric boundary layer*. Cambridge, UK: Cambridge University Press.

Giovannini, L., Zardi, D., & de Franceschi, M. (2011). Analysis of the urban thermal fingerprint of the city of Trento in the Alps. *Journal of Applied Meteorology and Climatology, 50*, 1145–1162.

Giovannini, L., Zardi, D., & de Franceschi, M. (2013). Characterization of the thermal structure inside an urban canyon: Field measurements and validation of a simple model. *Journal of Applied Meteorology and Climatology, 52*, 64–81.

Gousseau, P., Blocken, B., & van Heijst, G. J. F. (2011). CFD simulation of pollutant dispersion around isolated buildings: On the role of convective and turbulent mass fluxes in the prediction accuracy. *Journal of Hazardous Materials, 194*, 22–434.

Grimmond, C. S. B., & Oke, T. R. (1999). Aerodynamic properties of urban areas derived from analysis of urban surface form. *Journal of Applied Meteorology, 38*, 1261–1292.

Holton, J. R. (1992). *An introduction of dynamic meteorology*. New York: Academic Press.

Jacobson, M. Z. (2005). *Fundamentals of atmospheric modelling*. Cambridge: Cambridge University Press.

Jaroslawski, T., Perret, L., Blackman, K., & Savory, E. (2019). The spanwise variation of roof-level turbulence in a street-canyon flow. *Boundary-Layer Meteorology, 170*, 373–394.

Kastner-Klein, P., & Rotach, M. W. (2004). Mean flow and turbulence characteristics in an urban roughness sublayer. *Boundary-Layer Meteorology, 111*, 55–84.

Kent, C. W., Grimmond, S., Barlow, J., Gatey, D., Kotthaus, S., Lindberg, F., & Halios, C. H. (2017). Evaluation of urban local-scale aerodynamic parameters: Implications for the vertical profile of wind speed and for source areas. *Boundary-Layer Meteorology, 164*, 183–213.

Kim, J.-J., & Baik, J.-J. (1999). A numerical study of thermal effects on flow and pollutant dispersion in urban street canyons. *Journal of Applied Meteorology, 38*, 1249–1261.

Kim, J.-J., & Baik, J.-J. (2001). Urban street canyon flows with bottom heating. *Atmospheric Environment, 35*, 3395–3404.

Kim, J.-J., & Baik, J.-J. (2004). A numerical study of the effects of ambient wind direction on flow and dispersion in urban street canyons using the RNG k-E turbulence model. *Atmospheric Environment, 38*, 3039–3048.

Kovar-Panskus, A., Louka, P., Sini, J. F., Savory, E., Czech, M., Abdelqari, A., et al. (2002). Influence of geometry on the mean flow within urban street canyons—A comparison of wind tunnel experiments and numerical simulations. *Water, Air, & Soil Pollution: Focus, 2*, 365–380.

Lai, D., Karava, P., & Chen, Q. (2015). Study of outdoor ozone penetration into buildings through ventilation and infiltration. *Building and Environment, 93*, 112–118.

Leo, L. S., Thompson, M. J., Di Sabatino, S., & Fernando, H. J. S. (2016). Stratified Flow Past a Hill: Dividing Streamline Concept Revisited. *Boundary-Layer Meteorology, 159*, 611–634.

Li, W.-W., & Meroney, R. N. (1983). Gas dispersion near a cubical model building. Part I. Mean concentration measurements. *Journal of Wind Engineering and Industrial Aerodynamics, 12*, 15–33.

Liu, C.-H., Leung, D. Y. C., & Barth, M. C. (2005). On the prediction of air and pollutant exchange rates in street canyons of different aspect ratios using large-eddy simulation. *Atmospheric Environment, 39*, 1567–1574.

Louka, P., Belcher, S. E., & Harrison, R. G. (2000). Coupling between air flow in streets and the well-developed boundary layer aloft. *Atmospheric Environment, 34*, 2613–2621.

Lu, J., Arya, S. P., Snyder, W. H., & Lawson, R. E., Jr. (1997). A laboratory study of the urban heat island in a calm and stably stratified environment. Part I: Temperature field. *Journal of Applied Meteorology, 36*, 1377–1391.

Macdonald, R. W. (2000). Modelling the mean velocity profile in the urban canopy layer. *Boundary-Layer Meteorology, 97*, 25–45.

Martilli, A., Clappier, A., & Rotach, M. W. (2002). An urban surface exchange parameterisation for mesoscale models. *Boundary-Layer Meteorology, 104*, 261–304.

Martinuzzi, R, 1992. *Experimentelle Untersuchung der umströmung wandgebundener, rechteckiger, prismaticher hindernisse*. Ph.D. Dissertation, Universitat Erlangen-Nurnberg.

Martinuzzi, R., & Tropea, C. (1993). The flow around surface-mounted, prismatic obstacles placed in a fully developed channel flow: (data bank contribution). *Journal of Fluids Engineering, 115*, 85–92.

Mei, S. J., Hu, J. T., Liu, D., Zhao, F. Y., Li, Y., Wang, Y., & Wang, H. Q. (2017). Wind driven natural ventilation in the idealized building block arrays with multiple urban morphologies and unique package building density. *Energy and Buildings, 155*, 324–338.

Monin, A. S., & Obukhov, A. M. (1954). Basic laws of turbulent mixing in the atmosphere near the ground. *Trudy Geofiz. Inst. AN SSSR, 24*(151), 163–187.

Moonen, P., Defraeye, T., Dorer, V., Blocken, B., & Carmeliet, J. (2012). Urban Physics: Effect of the micro-climate on comfort, health and energy demand. *Frontiers of Architectural Research, 1*, 197–228.

Murakami, S. (1993). Comparison of various turbulence models applied to a bluff body. *Journal of Wind Engineering and Industrial Aerodynamics, 46–47*, 21–36.

Nardecchia, F., Di Bernardino, A., Pagliaro, F., Monti, P., Leuzzi, G., & Gugliermetti, L. (2018). CFD analysis of urban canopy flows employing the V2F model: Impact of different aspect ratios and relative heights. *Advances in Meteorology, 2018*, 2189234.

Oke, T. R. (1982). The energetic basis of the urban heat island. *Quarterly Journal of the Royal Meteorological Society, 108*, 1–24.

Oke, T. R. (1987). *Boundary layer climates* (2nd ed.). London: Routledge.

Oke, T. R. (1988). Street design and urban canopy layer climate. *Energy and Buildings, 11*, 103–113.

Ottosen, T.-B., Ketzel, M., Skov, H., Hertel, O., Brandt, J., & Kakosimos, K. E. (2019). Micro-scale modelling of the urban wind speed for air pollution applications. *Scientific Reports, 9*, 14279.

Pelliccioni, A., Monti, P., & Leuzzi, G. (2015). An alternative wind profile formulation for urban areas in neutral conditions. *Environmental Fluid Mechanics, 15*, 135–146.

Pichelli, E., Ferretti, R., Cacciani, M., Siani, A. M., Ciardini, V., & Di Iorio, T. (2014). The role of urban boundary layer investigated with high-resolution models and ground-based observations in Rome area: A step towards understanding parameterization potentialities. *Atmospheric Measurements Technology, 7*, 315–332.

Pournazeri, S., Princevac, M., & Venkatram, A. (2012). Rise of Buoyant Emissions from Low-Level Sources in the Presence of Upstream and Downstream Obstacles. *Boundary-Layer Meteorology, 144*, 287–308.

Ratti, C., Di Sabatino, S., & Britter, R. (2006). Urban texture analysis with image processing techniques: Winds and dispersion. *Theoretical and Applied Climatology, 84*, 77–90.

Ravanelli, R., Nascetti, A., Cirigliano, R. V., Di Rico, C., Leuzzi, G., Monti, P., & Crespi, M. (2018). Monitoring the impact of land cover change on surface urban heat island through Google Earth Engine: Proposal of a global methodology, first applications and problems. *Remote Sensing, 10*, 1488.

Rodi, W. (1995). Introduction to the numerical simulation approaches in wind engineering. In J. E. Cermak, A. G. Davenport, E. J. Plate, & D. X. Viegas (Eds.), *Wind climate in cities* (NATO ASI Series (Series E: Applied Sciences)) (Vol. 277). Dordrecht: Springer.

Rotach, M. W. (1999). On the influence of the urban roughness sublayer on turbulence and dispersion. *Atmospheric Environment, 33*, 4001–4008.

Roth, M., Oke, T. R., & Emery, W. J. (1989). Satellite-derived urban heat islands from three coastal cities and the utilization of such data in urban climatology. *International Journal of Remote Sensing, 10*, 1699–1720.

Salizzoni, P., Soulhac, L., & Mejean, P. (2009). Street canyon ventilation and atmospheric turbulence. *Atmospheric Environment, 43*, 5056–5067.

Salizzoni, P., Marro, M., Soulhac, L., Grosjean, N., & Perkins, R. J. (2011). Turbulent transfer between street canyons and the overlying atmospheric boundary layer. *Boundary-Layer Meteorology, 141*, 393–414.

Salvati, A., Coch Roura, H., & Cecere, C. (2017a). Assessing the urban heat island and its energy impact on residential buildings in Mediterranean climate: Barcelona case study. *Energy and Buildings, 146*, 38–54.

Salvati, A., Palme, M., & Inostroza, L. (2017b). Key parameters for urban heat island assessment in a Mediterranean context: A sensitivity analysis using the Urban Weather Generator Model. *IOP Conferences Series: Material Sciences and Engineering, 245*(8), 082055.

Salvati, A., Monti, P., Coch Roura, H., & Cecere, C. (2019). Assessing the urban heat island and its energy impact on residential buildings in Mediterranean climate: Barcelona case study. *Energy and Buildings, 185*, 162–179.

Santamouris. (2001). *Energy and climate in the urban built environment*. London, UK: James & James Ltd.

Santos, J. M., Reis, N. C., Jr., Goulart, E. V., & Mavroidis, I. (2009). Numerical simulation of flow and dispersion around an isolated cubical building: The effect of the atmospheric stratification. *Atmospheric Environment, 43*, 5484–5492.

Simpson, J. E. (1994). *Sea breeze and local winds*. Great Britain: Cambridge University Press.

Snyder, W. H. (1994). Downwash of plumes in the vicinity of buildings: A wind-tunnel study. In P. A. Davies & M. J. V. Neves (Eds.), *Recent research advances in the fluid mechanics of turbulent jets and plumes* (NATO ASI Series (Series E: Applied Sciences)) (Vol. 255). Dordrecht: Springer.

Soulhac, L., Perkins, R. J., & Salizzoni, P. (2008). Flow in a street canyon for any external wind direction. *Boundary-Layer Meteorology, 126*, 365–388.

Stewart, I. D., & Oke, T. R. (2012). Local climate zones for urban temperature studies. *Bullettin of the American Meteorological Society, 92*, 1879–1900.

Stull, R. B. (1988). *An introduction to boundary layer meteorology*. The Netherlands: Kluwer Academic Publisher.

Takimoto, H., Sato, A., Barlow, J. F., Moriwaki, R., Inagaki, A., Onomura, S., & Kanda, M. (2011). Particle image velocimetry measurements of turbulent flow within outdoor and indoor urban scale models and flushing motions in urban canopy layers. *Boundary-Layer Meteorology, 140*, 295–314.

Tominaga, Y., & Stathopoulos, T. (2009). Numerical simulation of dispersion around an isolated cubic building: Comparison of various types of k-ε models. *Atmospheric Environment, 43*, 3200–3210.

Tominaga, Y., & Stathopoulos, T. (2010). Numerical simulation of dispersion around an isolated cubic building: Model evaluation of RANS and LES. *Building and Environment, 45*, 2231–2239.

Valerio, G., Cantelli, A., Monti, P., & Leuzzi, G. (2017). A modeling approach to identify the effective forcing exerted by wind on a prealpine lake surrounded by a complex topography. *Water Resources Research, 53*, 4036–4052.

van Hooff, T., & Blocken, B. (2010). Coupled urban wind flow and indoor natural ventilation modelling on a high-resolution grid: A case study for the Amsterdam ArenA stadium. *Environmental Modelling & Software, 25*, 51–65.

Whiteman, C. D. (2000). *Mountain meteorology: Fundamentals and applications*. UK: Oxford University Press.

Xie, X., Huang, Z., & Wang, J. S. (2005a). Impact of building configuration on air quality in street canyon. *Atmospheric Environment, 39*, 4519–4530.

Xie, X., Huang, Z., Wang, J. S., & Xie, Z. (2005b). The impact of solar radiation and street layout on pollutant dispersion in street canyon. *Building and Environment, 40*, 201–212.

Zajic, D., Fernando, H. J. S., Calhoun, R., Princevac, M., Brown, M. J., & Pardyjak, E. R. (2011). Flow and turbulence in an urban canyon. *Journal of Applied Meteorology and Climatology, 50*, 203–223.

Zhou, Y., Guan, H., Huang, C., Fan, L., Gharib, S., Batelaan, O., & Simmons, C. (2019). Sea breeze cooling capacity and its influencing factors in a coastal city. *Building and Environment, 166*, 106408.